Molecular Vision 2022; 28:280-299 <http://www.molvis.org/molvis/v28/280>
Received 2 July 2021 | Accepted 2 September 2022 | Published 4 September 2022

Nestin contributes to laser choroidal and retinal neovascularization

Sofiane Miloudi,[1] Maud Valensi,[1] Mohamed El Sanharawi,[1] Marc M. Abitbol,[1,2] Francine Behar-Cohen,[1,3] Claudine Versaux-Botteri[1]

[1]Centre de Recherches des Cordeliers, UMR_S INSERM 1138, Équipe 17, Université Paris Cité, Université Paris Sorbonne Cité, Paris, France; [2]APHP, Hôpital Universitaire Necker-Enfants Malades, Paris, France; [3]APHP, Hôpital Universitaire Cochin-Hôtel Dieu, Paris, France

Purpose: Choroidal and retinal neovascularization plays an essential role in various ocular diseases. In this study, we examined the role of nestin in this process. Nestin is an intermediate filament protein known to play several roles, including as a marker of neural progenitor and proliferating endothelial cells.
Methods: We used Brown Norway rats, in which choroidal and retinal neovascularization was induced using intraocular laser impacts. The role of nestin was examined using angiography, western blot from the second to the 14th day after laser impacts, and intraocular injection of nestin siRNA. The localization of the protein was specified by co-immunoreactivity with glial fibrillary protein (GFAP), glutamine synthetase (GS), and von Willebrand factor (vWF).
Results: In the control retina, nestin was found principally in glial structures in the ganglion cell layer, as confirmed by nestin/GFAP immunolabeling. Two days after the laser impacts, the nestin expression extended to numerous radial processes at the site of the impacts. With Bruch's membrane ruptured, these processes penetrated into the choroid. Nestin immunolabeling remained high from the third to the seventh day but appeared reduced on the 14th day. The nature of these processes was not clearly defined, but co-immunolabeling with GFAP suggested that they were principally in activated Müller cells from the third day after the laser impacts. However, the co-immunoreactivity of nestin and GS, a marker of mature functional Müller cells, could be observable only from the seventh day. Nestin was also observed in some vascular cells, as demonstrated by the co-immunoreactivity of the protein with vWF in the choroid and retina. As observed on angiography, the numbers of choroidal and retinal blood vessels were significantly increased (principally on the seventh day) after the laser impacts. An intraocular injection of nestin siRNAs led to a significant decrease in the number of blood vessels.
Conclusions: Our results confirmed the presence of nestin in glial (e.g., astrocytes), reactive Müller, and endothelial cells. They demonstrated their critical involvement in a rat model of retinal and choroidal neovascularization experimentally induced using ocular laser impacts.

Although laser photocoagulation is used to treat the most frequent neovascular retinal diseases such as diabetic retinopathy (DR), occlusions of the central retinal vein, or exudative age-related macular degeneration (wet AMD) [1-4], it is also used for experimentally inducing injury to Bruch's membrane and for creating experimental choroidal neovascularization in animal models [1,5]. Indeed, when appropriate parameters are used for laser ray administration, the laser impacts break Bruch's membrane and induce subretinal neovascularization. These models and the hyperoxia/normoxia animal models associated with the induction of neovascularization are used for providing proofs of concept for anti-angiogenic molecules in preclinical studies of treatments focused principally on either tumoral and subretinal neovascularizations [6-10].

Correspondence to: Claudine Versaux-Botteri C, UMR_S INSERM 1138, Equipe 17, 15 rue de l'Ecole de Médecine, 75006, Paris, France. Phone: 0033144278175; email: claudine.botteri@sorbonne-universite.fr

Laser photocoagulation is believed to produce choroidal vascular malfunction because the high thermal energy causes rupture of Bruch's membrane and leads to ingrowth and/or remodeling of the choroidal and retinal vessels [11,12]. It also produces a local circumscribed area of retinal damage within which one can examine Müller cell changes [13].

After any retinal injury in experimental conditions, glial cells are activated and undergo reactive gliosis with increased an expression level of glial fibrillary acid protein (GFAP), which leads to overgrowth of outer Müller glial cell processes. Müller cells line up radially across the entire thickness of the retina. Among their multiple roles is the provision of mechanical support and nutrient supply, protection against toxic environments, and separation of nervous tissue from the vessels [14]. The growth of their processes outside the neural retina can sometimes create a physical barrier between the retinal pigment epithelium (RPE) and the photoreceptors [15]. In response to retinal injury, Müller cells appear to proliferate

and could dedifferentiate, as suggested by the presence of nestin [16-20].

Nestin is a component of the family of intermediate filaments (IFs). It was described as a neural stem/progenitor cell marker appearing during development [21,22] and is generally recognized as a marker of undifferentiated central nervous system (CNS) cells at the stage preceding the exit from the cell cycle. Its expression is downregulated when CNS progenitor cells differentiate into neurons or glial cells [23,24]. Moreover, nestin also appears to have angiogenic properties [25,26]. Endothelial cells in CNS tumors contain nestin [25,27], and its presence in the endothelium of vascular neoplasm in cancers suggests that it could constitute a marker of angiogenesis and neovascularization [28-30].

To accurately determine the retinal and choroidal cellular localization of nestin after laser impacts, we investigated the colocalization of the protein using GFAP (a marker for activated glial cells), glutamine synthetase (GS; a marker of fully differentiated adult Müller cells), and von Willebrand Factor (vWF; a marker of endothelial cells) at different times. Moreover, to clarify the functional role of nestin in neovascularization after krypton laser impacts, we performed an in vivo intravitreal injection of nestin small interfering RNA (siRNAs) to reduce the expression level of the protein. We demonstrated its direct involvement in the neovascularization induced by laser impacts using fluorescein angiography.

METHODS

Experimental procedures were performed in accordance with the European Communities Council Directive 86/609/EEC approved by local ethical committees and the ARVO statement for the Use of Animals in Ophthalmologic and Vision Research. Principles of laboratory animal care (NIH publication No. 85-23, revised 1985) and specific national laws were followed where applicable.

We used male Brown Norway rats obtained from Harlan Laboratories BV (the Netherlands). For each method used in this study (induction of choroidal neovascularization by laser impacts to break Bruch's membrane, intraocular injection of nestin siRNAs, in vivo fluorescein angiography, western blotting, and immunohistochemistry), the number of animals used was specified in the description of each experimental condition.

Induction of experimental choroidal and retinal neovascularization by laser: Rats were anesthetized with an intraperitoneal injection of 75-mg/kg Ketamine Virbac 1000 (Wissous-France) and 0.5-mg/kg Largactil (Sanofi-Aventis, Paris, France). Their pupils were dilated with 2 mg/0.4 ml of 1% Tropicamide Faure (Novartis Pharma, Rueil-Malmaison, France). The animals received eight krypton laser impacts in their right eye. The laser device used was the Ophthalmo Quantel Medical Viridis 532 nm (Clermont-Ferrand, France) mounted on a slit-lamp BQ 900 (Haag-Streitt–Schweiz, Koeniz, Switzerland) totally adapted for rat investigations. It created eight laser burns around the optic nerve. Each laser impact had a diameter of 50 µm and a power of 175 mW over 100 ms. The spots were performed at a distance of 1–2 disc diameters from the optic nerve. A glass coverslip was used as a contact lens during the laser ray delivery. The laser application resulted in a bubble indicative of Bruch's membrane rupture.

siRNA delivery: The selective silencing of the nestin gene expression was accomplished with intravitreal administration of nestin siRNAs and classes of double-stranded RNA molecules with specific sequences targeting nestin (ref. GenBank NM_012987). The selected siRNAs were as follows: sequence 1, position 2843–2501: forward 5′-GAG AUU UCU GAU UCU CUC UdT dT-3′ and reverse 5′-AGA GAG AAU CAG AAA UCU CdT dT-3′; sequence 2, position 2811–2829: forward 5′-UGG UCC UCC UCU UCU GGA GdT dT-3′ and reverse 5′-CUC CAG AAG AGG AGG ACC AdT dT-3′; sequence 3, position 3536–3554: forward 5′-GCU GAC UGU CCU CUA CCC UdT dT-3′ and reverse 5′-AGG GUA GAG GAC AGU CAG CdT dT-3′. Nestin siRNAs were synthetized by Eurogentec (Liège, Belgique).

In some experiments, the injection of siRNAs was coupled with the fluorophore cyanine 3 (cy3) to enable tracking of siRNAs in the eye. TransIT-TKO was introduced in 2001 and was the first commercially available siRNA transfection reagent. Its efficacy has been first demonstrated by Amarzguioui M et al in 2006. Thus, we followed the protocol recommended by the company Mirus (Mirus Bio, Madison, WI) and Amarzguioui et al [31] and described below. Nestin siRNAs were dissolved in a Transit-TKOreagent (Mirus Bio, Madison, WI) in accordance with the following protocol: 20 µM siRNA was combined with 5 µl of a Transit-T in vivo polymer solution in 10 µl of H_2O and incubated for 5 min at room temperature. Then, 190 µl of a Transit-T in vivo delivery solution was added to the preparation just before the intravitreal injection.

The rats subjected to laser impacts received an intravitreal injection of 3 µl of the siRNA preparation in the right eye. The first siRNA injection was administered just after the laser impacts and injections were renewed every 4 days because of the very fast degradation rate of the siRNAs. Results were compared with those obtained from the total control animals without any injection. Five animals for each

condition (nestin siRNAs and no injection) were sacrificed on the second, seventh, and 14th days after laser treatment.

In vivo fluorescein angiography: To visualize the retinal and choroidal vessels after the laser impacts and nestin siRNA injection, we performed in vivo angiography of the right eye on the second, seventh, and 14th days (five rats for each stage and each condition) after laser treatment. Control rats of the same age were also examined. The animals were anesthetized with intraperitoneal injection of 40-mg/kg Ketamine Virbac 1000 (Wissous, France). Then, 0.1-ml 10% fluorescein (Laboratoires SERB, Paris, France) associated with 0.02-ml infracyanine (Laboratoires SERB) diluted at 25 mg/10 ml in saline buffer was injected in the tail vein of the anesthetized rats. Pupil dilation was performed with a drop of 1% tropicamide ophthalmic solution (Akorn, Lake Forest, CA).

The ocular fundus was examined with a confocal scanning laser ophthalmoscope (Heidelberg Engineering, Heidelberg, Germany). The neovascularization areas were quantified using the Fij/Image J software. After opening a picture in ImageJ, we measured the number of vessels by the mean gray value in the Analysis part of the program. The vessel staining with fluorescein demonstrated that the bigger the vessel, the whiter the color. On the other hand, a lack of staining resulted in a black picture. We compared the values of the two groups at once (control/laser only and laser only/laser associated with nestin siRNAs) using the Mann-Whitney test.

Western blot: To verify the effect of nestin siRNAs on the nestin protein concentration, we performed a western blot analysis on all categories of the animals used (five rats for each category and stage). The animals were euthanized with a lethal inhalation of CO_2 always at the same time of day to reduce possible circadian variations in protein concentrations. The right eyes of all animals (control and treated) were enucleated on the second, seventh, and 14th days after the laser impacts. Ocular tissue was taken and placed in a specific buffer for the extraction of cytoskeletal proteins containing 10 mM Tris (pH 7.4), 100 mM NaCl, 1 mM ethylenediaminetetraacetic acid (EDTA), 1 mM ethylene glycol-*bis* (2 aminoethylether)-*N*,*N*,*N*′,*N*′-tetra acetic (EGTA), 1% Triton X-100, 10% glycerol, and 0.5% deoxycholate. Tris, NaCl, EDTA, EGTA, and deoxycholate were provided by Sigma-Aldrich-Merck (L'Isle d'Abeau-Chenes, France).

The samples were sonicated and centrifuged at 16,000 ×*g* for 30 min at 4 °C. The supernatant was collected, diluted in Laemmli buffer, and loaded (at a volume of 2 µl) onto 8% polyacrylamide gels (Invitrogen, Paris, France). After 1 h of electrophoresis, proteins were transferred (1.5 h at 150 V) to a poly-vinylidene difluoride membrane (Millipore, Guyancourt, France), blocked 2 h at room temperature in Tris-buffered saline containing 5% skim milk, and then incubated overnight with a goat polyclonal nestin antibody (ref. AF2736, Bio-Techne, Lille, France) diluted at 1:500 and with a rabbit β-actin antibody diluted at 1:7,500 (ref. A2103, Sigma-Aldrich, St. Quentin Fallavier, France). The β-actin antibody was used as an internal control. Membranes were finally incubated with a secondary peroxidase-conjugated anti-goat antibody diluted at 1:7,500 (ref. PI 9500, Vectorlabs, Eurobio Scientific, Les Ulis, France) or a secondary peroxidase-conjugated anti-rabbit antibody diluted at 1:20,000 (ref. PI 1000, Vectorlabs, Eurobio Scientific). The enzymatic activity of peroxidase was detected using the ECL + kit (General Electric Healthcare Europe GmBH, Velizy-Villacoublay, France). The intensity of labeling was observed with Image Quant LAS 4000 (General Electric Healthcare Europe GmBH) and measured with the ImageJ software, version 1.47c [32].

Immunohistochemistry: As for the western blot experiment, the control rats and animals subjected to laser impacts were euthanized with a lethal inhalation of CO_2 on the second, third, seventh, and 14th days after laser photocoagulation (with the addition of a third day as the time point to follow-up the activation of Müller cells). Moreover, nestin immunolabeling was realized on the 45th day after laser impact to observe tissue healing (Appendix 1). For each stage, the right eyes of six rats (three control rats and three rats with laser impacts, for a total of 24 rats) were enucleated, fixed in 4% paraformaldehyde for 24 h, cryoprotected in phosphate-buffered saline (PBS) containing 30% sucrose for 24 h, and embedded in a Tissue Tek OCT Compound (Sakura Finetek, Torrence, CA). The tissue sample was then frozen and sliced into 12-µm sections using a cryostat CM3050S (Leica Biosystems, Wetzlar, Germany). Sections that showed laser impacts were systematically collected and further processed. To visualize the global morphology of the retina, some slides were stained for 3 min with 4'6-diamino-2-phenylindole (DAPI) solution diluted at 1:6,000 (Sigma-Aldrich), washed twice in PBS, and mounted in glycerol/PBS (1:1). For immunohistochemistry, the tissue sections were incubated in PBS containing 0.1% Triton X-100 and 10% fetal calf serum (PBST) for 1 h, and then incubated overnight at 4 °C with primary antibodies diluted in PBST. The following antibodies were used: 1) goat polyclonal antibody anti-nestin (1:400, ref. AF2736, Bio-Techne), 2) mouse monoclonal antibody anti-GFAP (1:500, ref. MA5-15086, Thermo Scientific, Illkirch, France), 3) mouse monoclonal antibody anti-GS-clone GS-6 (GS 1:300, ref. MAB 302, Millipore, Guyancourt, France), and 4) rabbit polyclonal antibody anti-vWF (1:300, ref. A0082, Dako, Santa Clara, CA). Primary antibodies were visualized using the appropriate secondary fluorescent antibodies conjugated

to Alexa-488 or Alexa-546 (Life Technology, Villebon sur Yvette, France) diluted at 1:200 in PBS and incubated at room temperature in darkness for 1 h. The identity of nestin-immunopositive cells was studied through coimmunolabeling with anti-GS, anti-GFAP, or anti-vWF antibodies. Tissue sections were mounted in a fluorescent mounting medium (Dako) and viewed and photographed with a fluorescence microscope (BX51, Olympus, France). Staining was performed on a minimum of three independent samples. Negative controls were made by omitting the primary antibody. In this case, no evident immunolabeling was observed.

Tissue samples from photocoagulated and control eyes injected with siRNA were also collected. Some sections were stained only with DAPI, whereas others were incubated in anti-nestin antibody, as specified above.

Statistical analysis: For all comparisons, the Mann-Whitney test was used. The samples were considered significantly different from each other when the p value was <0.05.

RESULTS

Immunohistochemical expression levels of nestin in the choroid and retina after the laser impacts: To better visualize the effects of the laser impacts on the retina and choroid, two images of different retinas for each condition and each stage are shown, one for DAPI staining and one for nestin immunohistochemistry. They were examined at the site of the laser impacts and at 150 µm from the laser impact, and in control animals without laser treatment. We chose to show all pictures taken from different retinal sections.

On the second day after the laser impacts, DAPI staining demonstrated that the retinal morphology was normal in the control animals and at 150 µm from the laser impacts (Figure 1A,C). Nestin immunolabeling was observed in probable glial cells within the ganglion cell layer (GCL) and sometimes in rare radial processes crossing the thickness of the retina. It was also found in cells in some structures similar to the retinal and choroidal blood vessels (Figure 1B,D). In the retina subjected to laser impacts, DAPI staining revealed areas of damage and juxtaposed choroid corresponding to the zone of the laser impacts. These results showed a disruption of the RPE and Bruch's membrane and an apparent invasion of some retinal cell bodies into the choroid (Figure 1E). Nestin immunolabeling appeared intense at the site of the rupture. Within the neural retina, staining was observed in the radial process end feet of the presumptive Müller cells and structures such as blood vessels. Immunolabeling was also found mostly at the choroidal level (Figure 1F).

On the third day, the retinal and choroidal architecture in the control retina and at 150 µm from the lesion appeared not modified for the nestin immunoreactivity (Figure 1G–J). After the laser treatment, the rupture in Bruch's membrane was clearly observed with DAPI coloration. The lesion was larger than on the second day, and the invasion of the choroid by the outer retina was confirmed (Figure 1K). Nestin immunoreactivity was strong in the radial processes in the laser-damaged retinal and choroidal regions. It was also observed in some parts of the structures similar to blood vessels (Figure 1L).

On the seventh day after laser use, the retinal morphology and nestin expression at the periphery of the laser impacts and in the control animals appeared morphologically normal (Figure 1M–P). At the site of the lesion, evagination of retinal tissue into the choroid was always present (Figure 1Q). Nestin immunoreactivity was seen in radial retinal processes and the choroid. Structures such as blood vessels were always partially immunolabeled. The staining was very strong and concentrated in scar tissue at the site of the laser impact. The formation of edematous swelling within the retina and choroid was suspected (Figure 1R).

On the 14th day after the laser impacts, as in earlier stages, no morphological changes were observed in the control retina and in areas close to the periphery of the laser impacts (Figure 1S–V). At the site of the lesion, a scar between the retina and choroid appeared to be confirmed. The outer retina began to reform, although partial cellular disorganization was still observed (Figure 1W). Nestin immunoreactivity in the radial processes was always clearly detected in the retina at the site of laser-induced lesion, but their number appeared considerably reduced, as was also true for immunolabeling in the choroid. Structures similar to retinal blood vessels were still partially labeled in the retina and choroid (Figure 1X).

On the 45th day after the onset of the lesion, at the site of the laser injury, the retina and choroid were always partly disorganized, and nestin expression continued to be observed in the radial processes. For the control retina and the retina at 150 µm from the site of impact, no change was observed (Appendix 1).

Cellular localization of nestin: To accurately determine the cellular localization of nestin in choroidal and/or retinal tissue, we investigated the colocalization of nestin with GFAP, GS, and vWF. As no major changes were found in the control rats and at 150 µm from the laser impact at all examined stages, we chose to present only the results observed on the seventh day post impact (when the retina displayed the most important abnormalities in the area of the laser impact). For

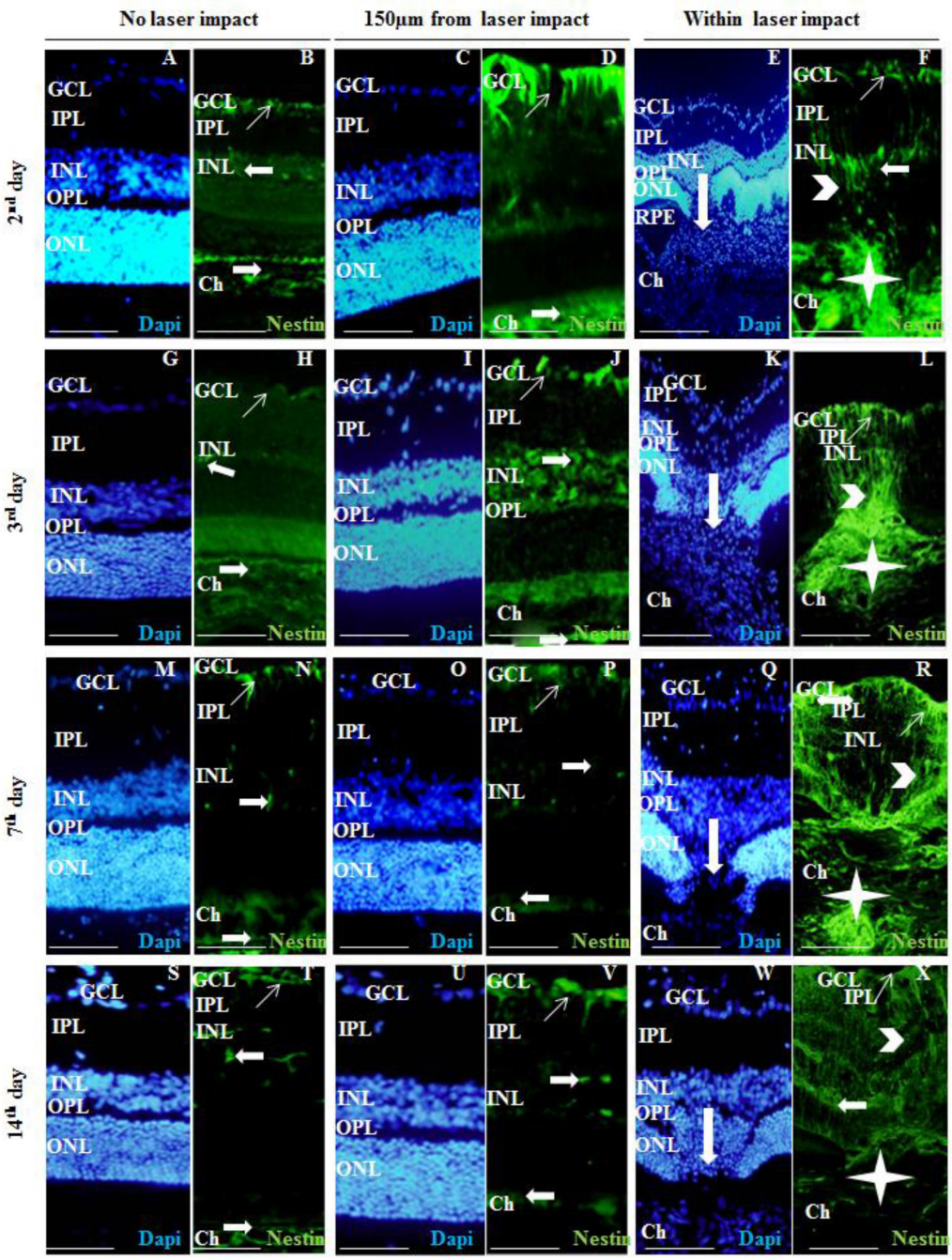

Figure 1. Histological pictures of the retina and choroid in the rats not treated with krypton laser impact, at a distance of 150 µm from the site where laser impact was to be applied and at the site of impact. Immunofluorescent labeling with DAPI (blue) and nestin (green) is shown. **A, C, G, I, M, O, S, and U**: No morphological changes can be observed in the control rats not treated with laser impact and at 150 µm from the site of laser impact, as observed with DAPI staining. Nestin immunostaining can be seen in the processes of astrocytes and in the probable end feet of Müller cells located mostly in the GCL (thin arrow). **B, D, H, J, N, P, T, and V**: Blood vessels are also located in the retina and choroid (horizontal large arrow). **E, K, Q, and W**: At the impact, DAPI labeling demonstrated that retinal morphology is greatly disrupted in the outer retina at all stages examined, with cells of the ONL entering the choroid (large vertical thick arrow), especially evident on the second and third days after laser impact. **F**: Nestin immunostaining was observed from the second day in glial cells in the GCL (thin arrow), in the retinal radial processes (horizontal large arrow), and in the choroidal processes (large star). The immunolabeling remained intense on the **L**: third day and **R**: seventh day, when an edema appeared to start to form (bold upper sign), but was decreased on the **X**: 14th day. Scale bars correspond to 50 µm. All pictures were taken from different retinal sections. GCL: ganglion cell layer, IPL: inner plexiform layer, INL: inner nuclear layer, OPL: outer plexiform layer, ONL: outer nuclear layer, Ch: choroid.

the rats that received laser impacts, we presented the results on the second, third, seventh, and 14th days after the impact.

Retina without laser impact: In the retina without laser impact, GFAP staining was detected principally in astrocytes within the GCL. Some immunolabeling was occasionally found in the outer plexiform layer (OPL; Figure 2A). Nestin was observed in the same types of cells (Figure 2B). GFAP/nestin coimmunolabeling confirmed that nestin and GFAP were localized in numerous glial cell bodies and processes (Figure 2C). GS (Figure 2D) was clearly detected in mature Müller cells (Figure 2E). GS/nestin co-immunolabeling was rarely observed in cells in the GCL but never in the radial processes and structures similar to blood vessels (Figure 2F). vWF (Figure 2G) was observed in the choroidal and retinal blood vessels. Nestin immunolabeling was detected in cells in the GCL and in structures like blood vessels in the retina and choroid (Figure 2H). Some vWF/nestin co-immunolabeling was observed in the retina and choroid (Figure 2I), so nestin was observed in some blood vessels.

Retina at 150 µm from the site of the laser impact: At 150 µm from the site of the laser impact, GFAP was found in astrocytes in the GCL and choroid. Some radial processes appeared to be also immunolabeled in the retina (Figure 3A). Nestin was detected in probable glial cells and processes in the GCL (Figure 3B). An increased number of immunolabeled radial processes was sometimes observed. GFAP/nestin co-immunolabeling was found in cells in the GCL. In the choroid, immunolabeling allowed the detection of glial cells (GFAP/nestin co-immunolabeling) and possible endothelial cells (only nestin immunolabeling; Figure 3C). GS was identified in the end feet and radial processes of physiologically mature retinal Müller cells (Figure 3D). Nestin was present in the cells with radial processes and cells in the choroid (Figure 3E). The GS/nestin co-immunolabeling was rarely observed in the GCL, whereas the choroidal structures were only labeled by nestin (Figure 3F). vWF was found in blood vessels in the retina and choroid (Figure 3G). In the retina, nestin immunolabeling was detected in cells in the retinal GCL, in some radial processes, and in blood vessels. It was also observed in choroidal blood vessels (Figure 3H). vWF/nestin co-immunoreactivity was sometimes observed partially overlapping in some retinal and in choroidal blood vessels (Figure 3I).

Retina at the level of the laser impact: In the area of the laser impact, on the second day after laser administration, GFAP appeared to be moderately upregulated at the site of the laser impact (Figure 4A–L). In the retina, GFAP immunoreactivity was found principally in astrocytes in the OPL and GCL and in some processes in the retina (Figure 4A). Nestin was observed in the GCL and retinal radial processes. Immunolabeling was also observed in processes along the path of the laser beam within the RPE and choroid (Figure 4B). Co-immunolabeling demonstrated the localization of nestin with GFAP only in glial cells in the GCL and OPL (Figure 4C). On the third day after laser administration, GFAP immunoreactivity was now clearly detected in astrocytes in the GCL and in numerous radial processes of activated Müller cells in the retina. These processes entered massively into the choroid (Figure 4D).

Nestin appeared to be observed in the same type of structures (Figure 4E). Nestin/GFAP co-immunolabeling confirmed that these two proteins were partially colocalized in processes in the GCL and in radial processes in the retina and choroid (Figure 4F). On the seventh day post laser administration, GFAP was always detected in the same retinal structures, principally in radial processes at the site of the laser impact. However, their entry into the choroid appeared restricted (Figure 4G). Nestin immunoreactivity presented the same distribution as GFAP (Figure 4H). Nestin/GFAP co-immunolabeling confirmed that these two proteins were now localized in numerous retinal radial processes of presumptive reactive retinal Müller cells. In the choroid, the colocalization appeared to be maintained, though less importantly than in the retina (Figure 4I).

On the 14th day after laser delivery, GFAP was always observed in radial processes at the site of the laser impact, but their number appeared to be reduced. They were present only in the neural retina between the GCL and the OPL, without any passage into the choroid probably because of scar formation. However, GFAP immunolabeling was still detectable in the choroid in probable astrocytes (Figure 4J). Nestin immunoreactivity presented the same pattern as that observed with GFAP immunolabeling (Figure 4K). Except in some structures found in the GCL, nestin and GFAP were coexpressed in most radial processes of activated Müller cells and in the GCL and choroid (Figure 4L).

On the second day after the laser impact, GS was observed in disorganized Müller cells confined within the retinal layers. Even though the outer retina appeared open at the site of the laser impact, no penetration of Müller cell processes into the ruptured RPE and choroidal layers could be seen (Figure 5A). Nestin was observed in the cells in the GCL and some radial processes (Figure 5B). GS/nestin co-immunolabeling was observed rarely in the GCL but never in functionally mature Müller cells (Figure 5C).

On the third day after laser administration, GS immunolabeling remained localized in Müller cells positioned only within the retina (even at the site of the laser impact),

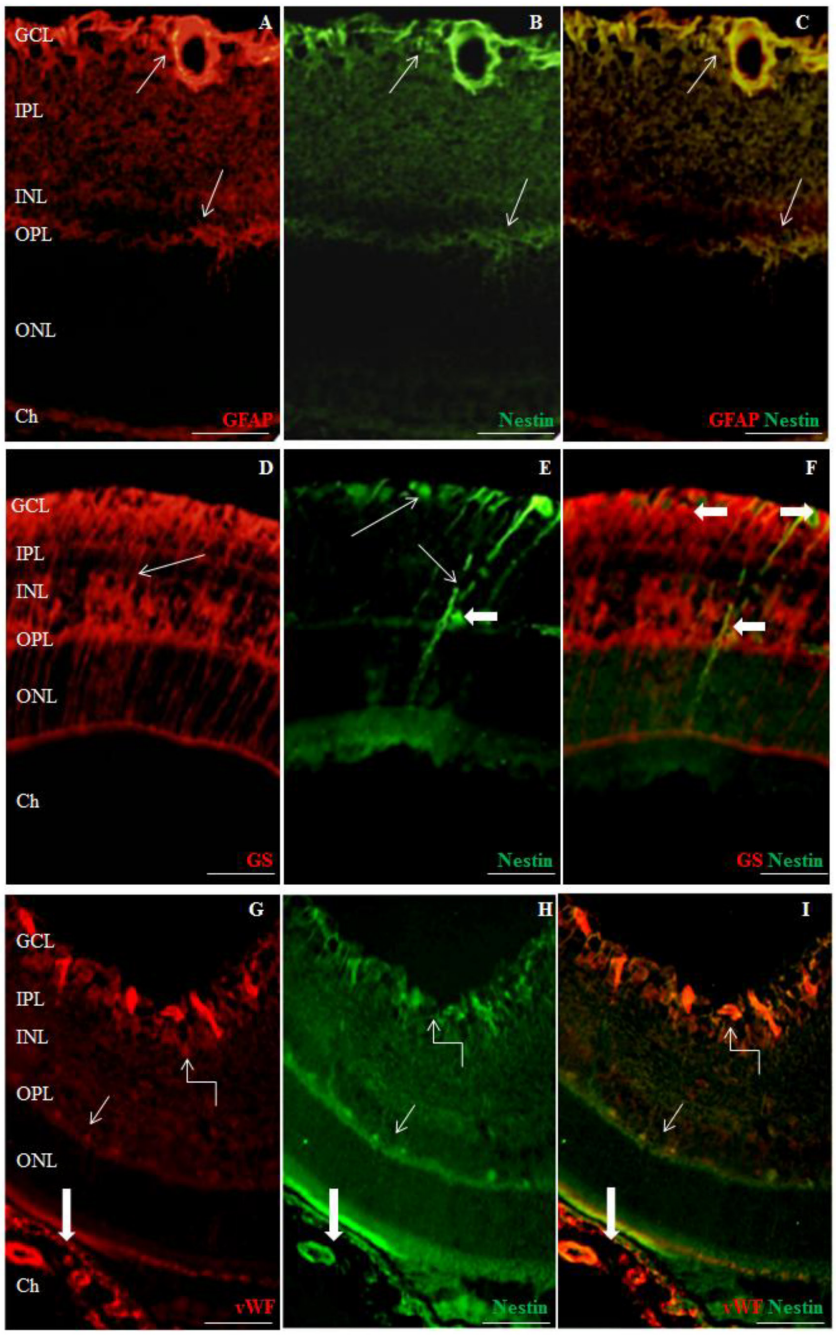

Figure 2. Retinal and choroidal nestin (green) co-immunolabeling with glial fibrillary acidic protein (GFAP, red), glutamine synthetase (GS, red), or von Willebrand factor (vWF, red) in the control retina on the seventh day post laser treatment. **A–C**: GFAP (red) and nestin (green). **A**: GFAP is present in astrocytes (upward thin arrow) and around some blood vessels (thick arrow) in the GCL and OPL. **B**: Nestin was detected in cells in the same retinal layers where the GFAP was detected. **C**: These results were confirmed by co-immunolabeling with nestin/GFAP. **D–F**: GS (red) and nestin (green). **D**: GS immunoreactivity can be observed in Müller cells (upward thin arrow). **E**: Nestin was detected in cells (probably in quiescent astrocytes) in the GCL (upward thin arrow) and rarely in some cells with radial processes (downward thin arrow). Some blood vessels appeared also partially labeled (leftward thick arrow). **F**: Nestin/GS co-immunolabeling is never observed in functional mature Müller cells (leftward thick arrow) and blood vessels (rightward thick arrow). **G–I**: vWF (red) and nestin (green). **G**: vWF immunolabeling was found in blood vessels in the retina (downward thin arrow and upward "plug" arrow) and choroid (downward thick arrow). **H**: Nestin immunolabeling was observed in the GCL (downward thin arrow and upward "plug" arrow), in the OPL (thin arrow), and at the choroid level (downward thick arrow). **I**: vWF/nestin co-immunolabeling was found in the GCL (upward "plug" arrow), in the OPL (downward thin arrow), and in the choroid (downward thick arrow). Scale bars correspond to 50 µm. GCL: ganglion cell layer, IPL: inner plexiform layer, INL: inner nuclear layer, OPL: outer plexiform layer, ONL: outer nuclear layer, Ch: Choroid.

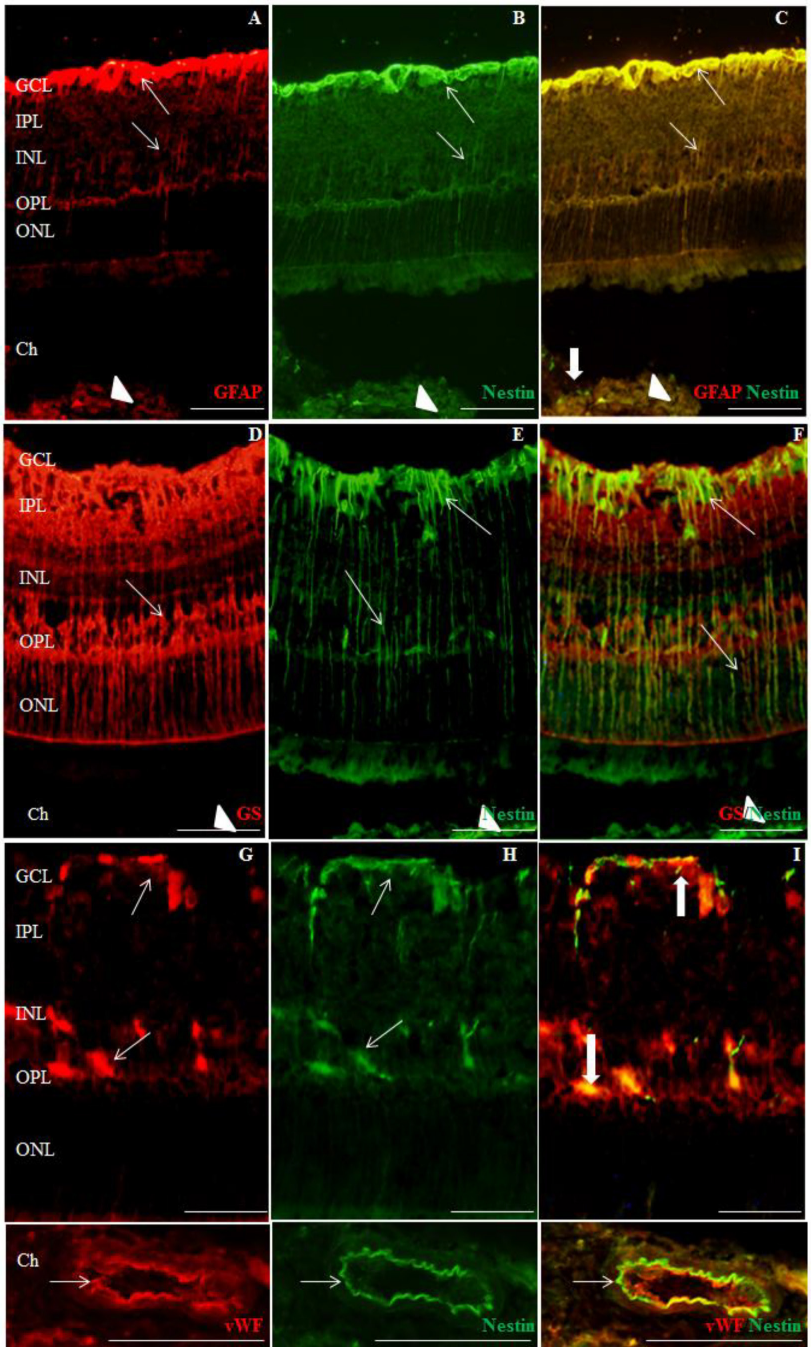

Figure 3. Retinal and choroidal nestin (green) co-immunolabeling with glial fibrillary acidic protein (GFAP; red), glutamine synthetase (GS; red), or von Willebrand Factor (vWF; red) at 100/150 µm from the site of the laser impact in the retina on the seventh day. **A–C**: GFAP (red) and nestin (green). **A**: GFAP immunoreactivity is present in astrocytes (thin arrow), around blood vessels (upward thick arrow) in the GCL, in the radial processes in the thickness of the retina (upward thin arrow), and in the choroid (arrowhead). **B**: Nestin is found in the same structures where GFAP is found. **C**: These results are confirmed by the co-immunolabeling GFAP/nestin. However, some structures (probably blood vessels) could only be immunolabeled by nestin (downward thick arrow). **D–F**: GS (red) and nestin (green). **D**: GS immunoreactivity can be observed in Müller cells (thin arrow) and sometimes at the choroidal level (arrowhead). **E**: Nestin is found in in the GCL (upward thin arrow), in the radial processes in the thickness of the retina (downward thin arrow), and in the choroid (arrowhead). **F**: Partial GS/nestin co-immunolabeling is rarely and partially observed in the radial processes (downward thin arrow) and GCL (upward thin arrow). No co-immunolabeling was found in the choroid (arrowhead) and probably in blood vessels at the choroidal level (arrowhead). **G–I**: vWF (red) and nestin (green). **G**: vWF can be observed in blood vessels throughout the retina (upward thin arrow) and choroid (horizontal thin arrow). **H**: Nestin was found in cells and processes in the retina (upward thin arrow). It was also detected in blood vessels in the retina (downward thin arrow) and choroid. **I**: Co-immunolabeling confirmed the presence of nestin and vWF in some blood vessels in the retina (thick arrow) and choroid. Scale bars correspond to 50 µm. GCL: ganglion cell layer, IPL: inner plexiform layer, INL: inner nuclear layer, OPL: outer plexiform layer, ONL: outer nuclear layer, Ch: choroid.

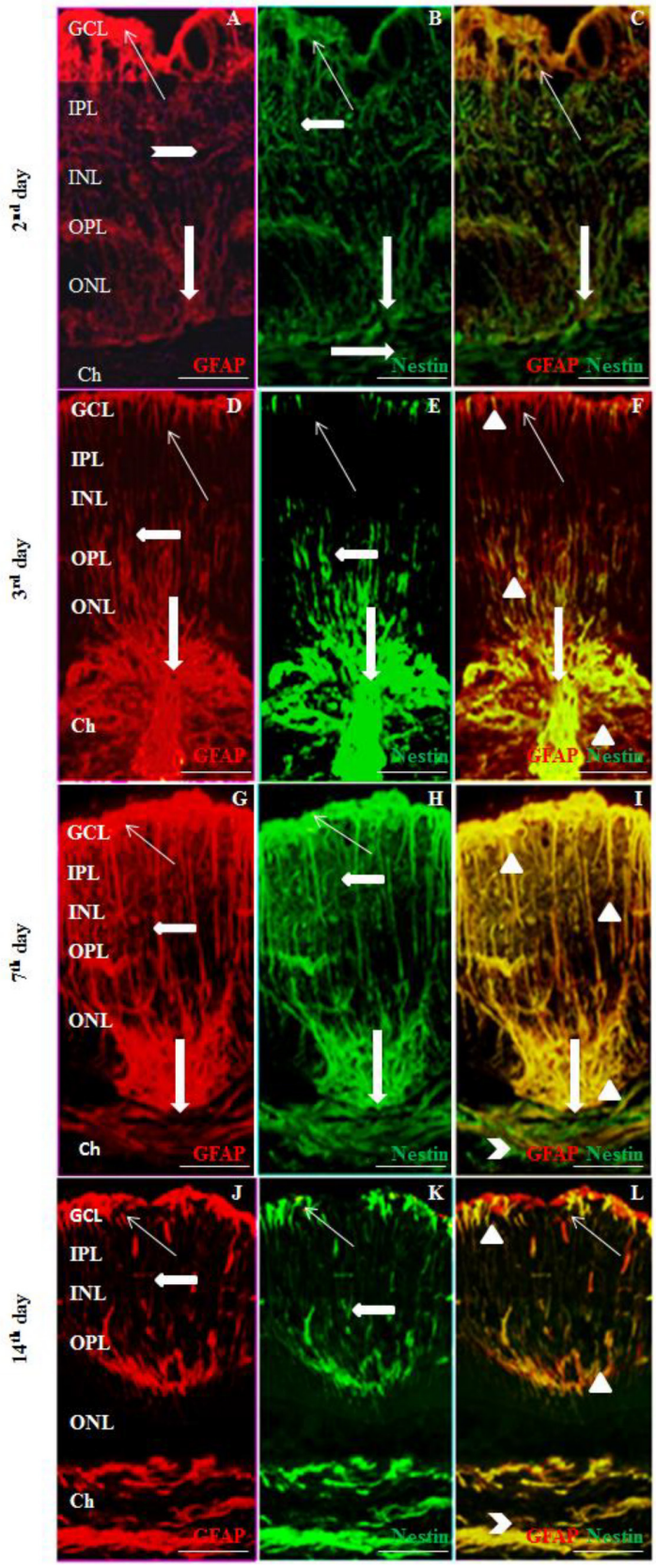

Figure 4. Glial fibrillary acidic protein (GFAP; red) and nestin (green) on the second, third, seventh, and 14th days after laser impact. On the second day post laser treatment, GFAP was observed mostly in the GCL (upward thin arrow) but was also found in some retinal processes (leftward thick arrow). **A**: The site of the laser impact started to appear (downward thick arrow), but no processes appeared to enter the choroid. Nestin was detected in the GCL (upward thin arrow) and retinal radial processes (leftward thick arrow). Some GFAP immunoreactive processes also appeared at the boundary between the retina and the choroid but did not enter the choroid (rightward thick arrow) **B**: Co-immunostaining confirmed these observations and allowed for the observation of a nestin/GFAP coexpression in the GCL (upward thin arrow), **C**: but not in the choroid. On the third day, the laser impact was clearly detectable, along with the ruptured Bruch's membrane (downward thick arrow). GFAP and nestin immunolabeling were observed in the **D**: GCL (upward thin arrow) and **E**: radial processes (leftward thick arrow), which clearly penetrated the choroid after the laser impact. **F**: GFAP/nestin co-immunostaining confirmed that some structures were co-immunolabeled in the retina and choroid (arrowhead). On the seventh day, **G**: GFAP and **H**: nestin labeling appeared in the same structures as those in the precedent stages in the GCL (upward thin arrow) and retinal radial processes (leftward thick arrow), but a scar began to form between the retina and the choroid (downward thick arrow), preventing the radial retinal processes to penetrate massively in the choroid. **I**: Co-immunostaining confirmed the colocalization of GFAP and nestin in cells in the GCL and radial processes in the retina (arrowhead) and a partial colocalization in the choroid (bold upper sign). On the 14th day, the morphology of the retina began to rebuild, and a scar between the retina and the choroid became clearly visible. However, no passage of radial retinal processes into the choroid was observed. GFAP and nestin immunolabeling are always detectable in the **J**: GCL (upward thin arrow) and **K**: retinal radial processes (leftward thick arrow), but their numbers appeared reduced. **L**: GFAP/nestin co-immunolabeling was observed in the GCL and retinal radial processes (arrowhead) as in the choroid (bold upper sign). GCL: ganglion cell layer, IPL: inner plexiform layer, INL: inner nuclear layer, OPL: outer nuclear layer, ONL: outer nuclear layer, Ch: choroid. Scale bars correspond to 50 µm.

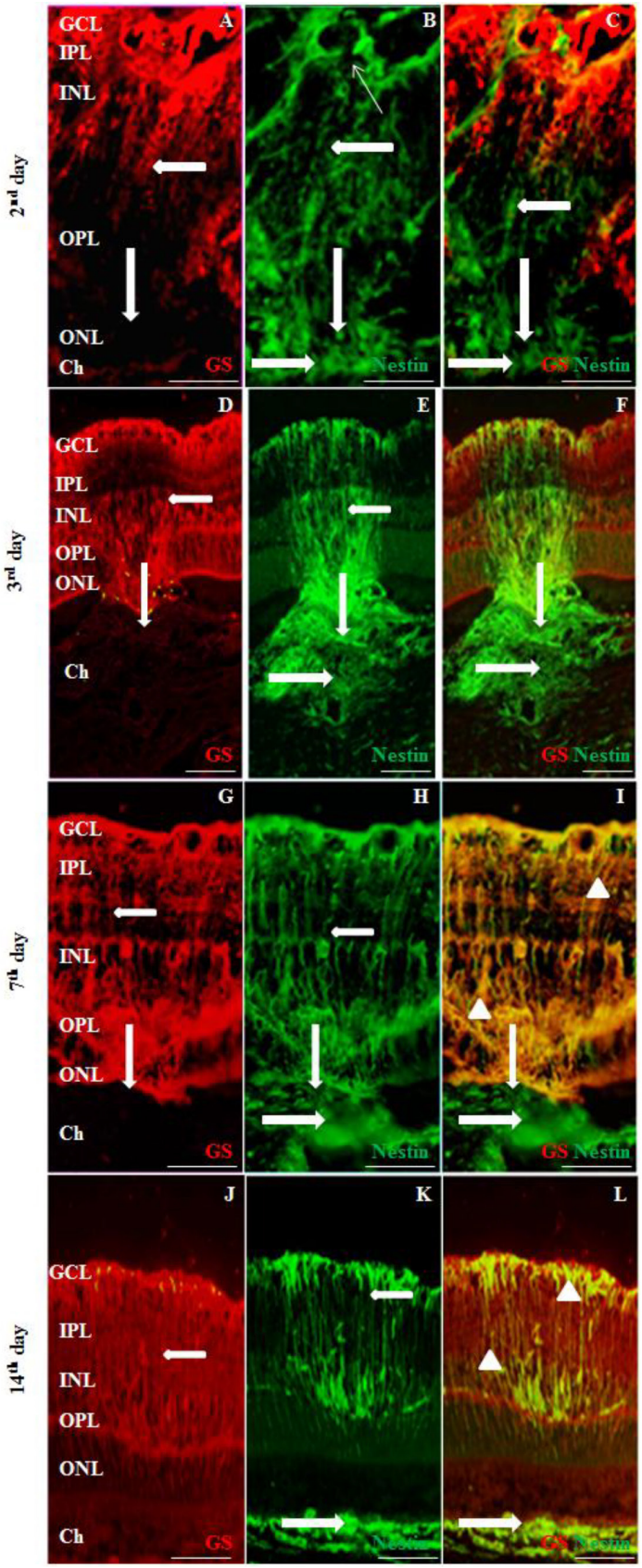

Figure 5. Glutamine synthetase (GS; red) and nestin (green) on the second, third, seventh, and 14th days after laser impact. **A**: On the second day post laser treatment, GS immunoreactivity was found in functionally mature Müller cells (leftward thick arrow) in spite of the local retinal morphology disturbance (downward thick arrow). **B**: Nestin immunoreactivity was observed in the GCL (upward thin arrow), as in the retinal radial processes (leftward thick arrow), which began to enter at the choroidal level (rightward thick arrow). **C**: GS/nestin co-immunolabeling demonstrated no evident colocalization between the nestin and the GS. On the third day, the laser impact was clearly detectable (downward thick arrow). **D**: GS was detected in Müller cells only in the retina (leftward thick arrow) despite the Brusch's membrane damage. **E**: Nestin immunolabeling was observed in the retinal radial processes (leftward thick arrow), clearly penetrating the choroid (rightward thick arrow). **F**: GS/nestin co-immunostaining demonstrated no evident colocalization of the proteins in the retina and choroid. **G**: On the seventh day, as for the previous stage, GS immunolabeling was found only in Müller cells in the retina (leftward thick arrow) despite the ruptured Bruch's membrane (downward thick arrow). Nestin immunoreactivity was observed in the radial processes in the retina (leftward thick arrow). **H**: As in the precedent stage, radial processes entered into the retina (downward thick arrow) and choroid (rightward thick arrow). **I**: GS/nestin co-immunolabeling demonstrated that some radial processes appeared partially co-immunolabeled in the retina (arrowhead), but no co-immunolabeling was observed at the choroidal level (rightward thick arrow). On the 14th day, the retinal architecture began to reform. **J**: GS immunolabeling is always found in Müller cells in the retina (leftward thick arrow). **K**: Nestin is still detected in some radial retinal processes (leftward thick arrow) and processes in the choroid (rightward thick arrow). **L**: GS/nestin co-immunostaining demonstrated a colocalization of these two proteins in the retinal radial processes (arrowhead) and confirmed the absence of GS at the choroidal level (rightward thick arrow). GCL: ganglion cell layer, IPL: inner plexiform layer, INL: inner nuclear layer, OPL: outer nuclear layer, ONL: outer nuclear layer, Ch: choroid. Scale bars correspond to 50 µm.

confirming that no functionally mature Müller cells had invaded the choroid (Figure 5D). Nestin was also mostly detected in the retinal radial processes and glial structures in the choroid (Figure 5E). Colocalization of GS and nestin in Müller cells was rarely observed in the radial processes, whereas no co-immunolabeling was found in the choroid (Figure 5F).

On the seventh day post laser administration, functionally mature GS immunoreactive Müller cells were only present in the retina, with their cell bodies aggregated near the outer nuclear layer (ONL), as for the previous stages (Figure 5G). Nestin was detected in the cells in the GCL and retinal radial processes, entering massively at the choroidal level (Figure 5H). The number of Müller cells co-immunolabeled with GS and nestin was increased in the retina (Figure 5I).

On the 14th day after laser delivery, GS immunolabeling was always found in Müller cells restricted to the retina. Some immunolabeling was observed at the choroidal level (Figure 5J). Nestin immunolabeling was observed in the retinal radial processes. However, these processes no longer entered into the choroid. This observation strongly supported the scar formation (Figure 5K). A co-expression of nestin and GS was now detected in most radial processes of functionally mature Müller cells, but never in the choroid (Figure 5L).

On the second day, vWF was detected in blood vessels in the retina and choroid at the site of the laser impact (Figure 6A). Nestin was detected in cells and processes, as in structures like blood vessels in the retina and at the choroidal level (Figure 6B). Co-immunolabeling demonstrated that some vascular vWF-containing cells were partially labeled for nestin at the level of the laser impact (Figure 6C). On the third day, vWF immunoreactivity was observed in blood vessels, with an increased density in the choroid (Figure 6D). Nestin was found in retinal radial processes penetrating into the choroid and structures similar to blood vessels (Figure 6E). Partial co-expression of vWF and nestin was also observed in some choroidal and retinal vessels at the level of the lesion (Figure 6F).

On the seventh day, vWF immunoreactivity remained detectable in retinal and choroidal blood vessels (Figure 6G). Nestin was always found in the same retinal and choroidal structures such as blood vessels (Figure 6H). An increased number of blood vessels co-expressed vWF and nestin in the retina and choroid (Figure 6I). On the 14th day, vessels immunolabeled with vWF antibody were always detected in the retina and choroid (Figure 6J). Nestin was always detected in the retinal GCL and radial processes, as in some structures present in the choroid (Figure 6K). A reduced number of blood vessels appeared partially colabeled with nestin and vWF antibodies, in the retina and choroid (Figure 6L).

siRNA administration: To examine the involvement of nestin after the laser-induced lesion, we performed an intravitreal administration of nestin siRNAs. To monitor and assess their distribution in the choroid/retina, fluorescent Cy3-labeled nestin siRNAs were used. At all stages, fluorescent signals were observed in nestin-containing cells localized in the retina and choroid of both the treated (Figure 7A) and control animals (Figure 7B), as presented on the seventh day after laser impact. siRNAs were detected primarily in the retinal GCL and choroidal areas, although they were sometimes also observed in the OPL. However, the presence of nestin siRNAs appeared clearly weaker in the controls than in the treated animals. Moreover, it was not uniform, revealing regions with high and low transfection levels.

Western blot: The intravitreal injection of specific nestin siRNAs led to a significant decrease of the retinal concentrations of nestin mostly on the second, seventh, and 14th days after laser impacts administration, as confirmed by western blot (Figure 8A-C, respectively). In the control animals not treated with laser, the nestin expression level did not change from the second to the 14th day.

Angiography: To measure the effect of siRNA nestin inhibition on ocular neovascularization, we used in vivo fluorescein angiography. With this technique, vessels could be visualized throughout the posterior pole of the eye. At all studied ages, the organization and density of blood vessels were not modified in the control animals, but several modifications were observed in those treated with laser. On the second day after the laser treatment, no new vessel growth could be seen in the posterior pole, whereas on the seventh day, hyperfluorescent neovessels could be observed crossing the ruptured retina and Bruch's membrane. On the 14th day after the onset of laser burn, neovessels were still detected, and most lesions contained a dense microvascular network that grew beyond the RPE. The intravitreal injection of nestin siRNAs considerably reduced the extent of the neovascularization, especially on the seventh and 14th days. However, though decreased, the extent and fluorescence intensity of the neovessels remained prominent at these post-laser stages (Figure 9A). These morphological results were confirmed by a statistical study (Figure 9B–D).

DISCUSSION

In this work, we observed the retinal and choroidal localizations of nestin and its involvement in neovascularization after laser impacts. Nestin is a type VI IF protein generally recognized as a marker of undifferentiated CNS progenitor

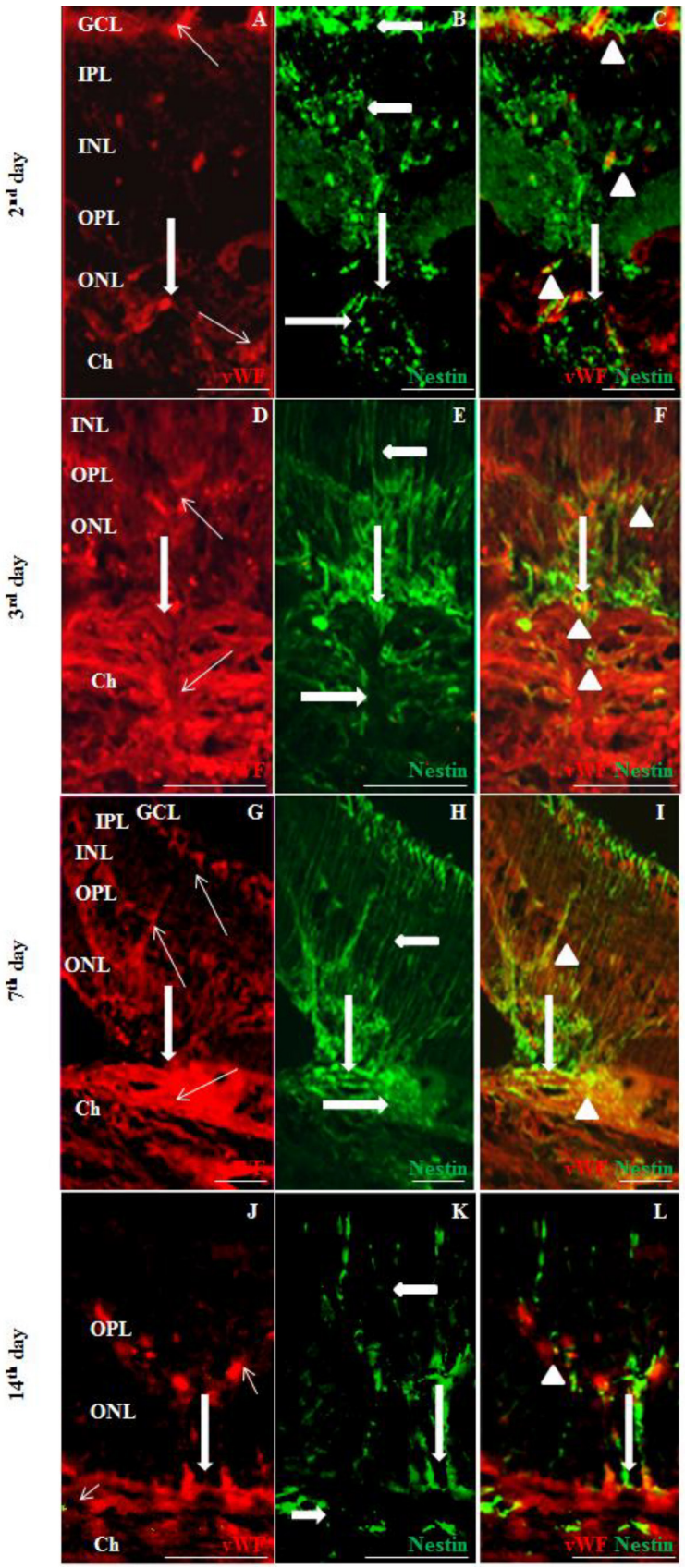

Figure 6. von Willebrand factor (vWF, red) and nestin on the second, third, seventh, and 14th days after laser impact. **A**: On the second day post laser impact, vWF expression was found in blood vessels in the retina (upward thin arrow) and choroid (downward thin arrow) at the site of the laser impact (downward thick arrow). **B**: Nestin immunoreactivity was found in the GCL and processes of the retina (leftward horizontal thick arrow) and choroid (rightward horizontal thick arrow). **C**: Some vWF and nestin co-immunolabeling can be observed in the retina and choroid (arrowhead). **D**: On the third day, as in the precedent stage, vWF expression was detected in blood vessels in the retina (upward thin arrow) and choroid (downward thin arrow) massively at the site of the laser impact (downward thick arrow). **E**: Nestin was detected in the retinal radial processes and blood vessels in the retina (leftward thick arrow) and choroid (rightward thick arrow), principally at the site of the laser impact (downward thick arrow). **F**: vWF/nestin co-immunolabeling confirmed that blood vessels were partially immunolabeled in the retina, as in the choroid (arrowhead). The same type of immunolabeling was found on the seventh and 14th days post laser treatment, with a progressive decrease in the number of nestin immunolabeling (**G–I** and **J–L**). GCL: ganglion cell layer, IPL: inner plexiform layer, INL: inner nuclear layer, OPL: outer nuclear layer, ONL: outer nuclear layer, Ch: choroid. Scale bars correspond to 50 µm.

cells at the stage that precedes exit from the cell cycle [21]. Sometimes associated with other intermediate filaments such as vimentin, nestin forms IF bundles in progenitor cells [33]. It is also thought to be responsible for maintaining structural cellular integrity. Moreover, it has been suggested that it could be involved in the positioning and functioning of subcellular organelles serving as a scaffold for kinases that regulate various functions such as proliferation, cell survival, and differentiation [34-38]. Nestin is regulated in a cell cycle-dependent manner, upregulated during the G1-S phase, when neural progenitor cells elongate, but declining in the G2-M phase, when the progenitor cells round up to undergo mitosis [39]. Also, it binds the Cdk5/p35 signaling complex and thereby works as an anti-apoptotic factor [40,41]. During development, it is associated with the migration and proliferation of immature neuronal and non-neuronal cells

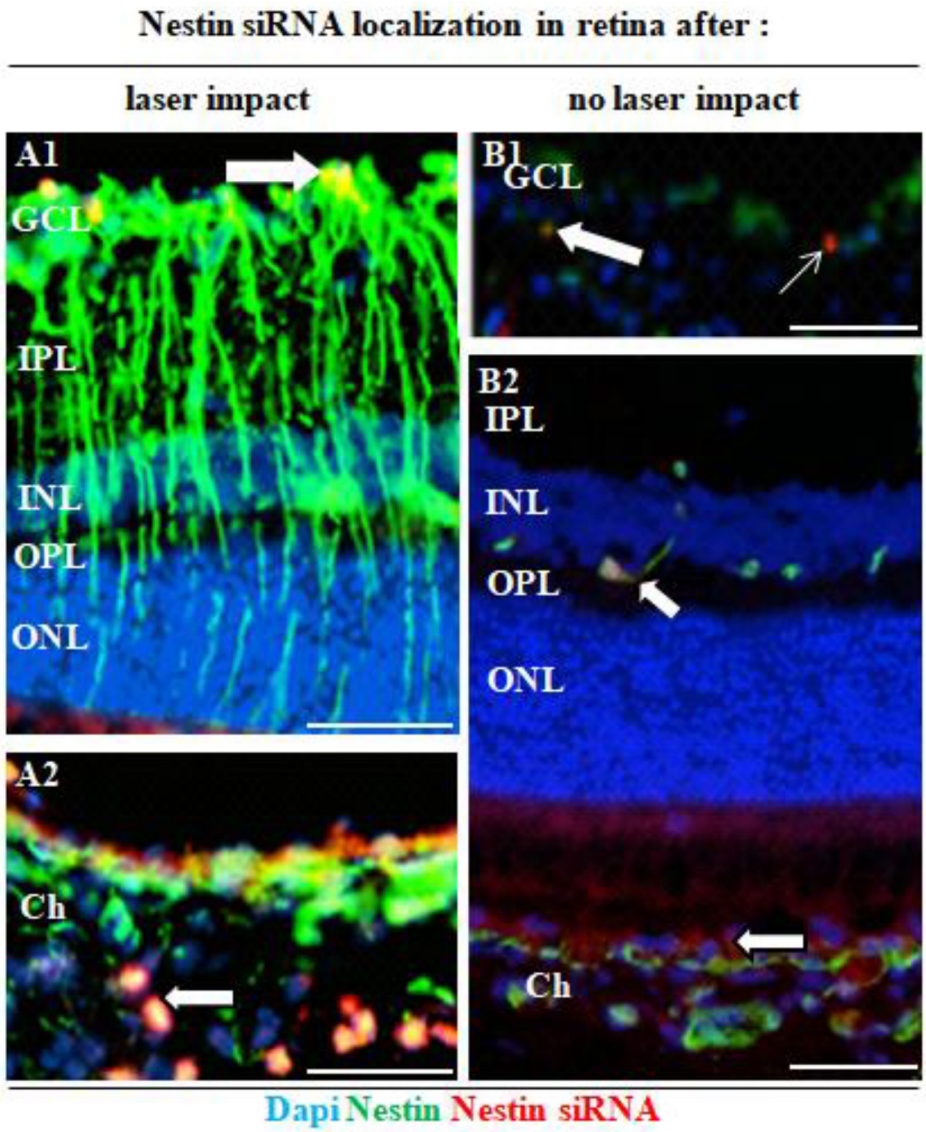

Figure 7. Localization of Cy3 fluorescent nestin siRNAs in the retina **A**: with and **B**: without laser impact. Nestin immunoreactivity is shown in green. In **A1**: the retina, on the seventh day after laser impact, nestin siRNAs were abundant in some nestin-immunoreactive cells in the GCL (rightward thick arrow) and **A2**: choroid (leftward thick arrow). In the control retina (retina without laser impact), nestin siRNAs were occasionally observed in the inner retina (leftward thick arrow), **B2**: blood vessels in the retina (upward thick arrow), and **B2**: choroid (leftward thick arrow). **B1**: Some siRNAs appeared not integrated in the retinal cells (rightward thin arrow). Scale bars correspond to 50 µm. GCL: ganglion cell layer, IPL: inner plexiform layer, INL: inner nuclear layer, OPL: outer plexiform layer, ONL: outer nuclear layer, Ch: choroid.

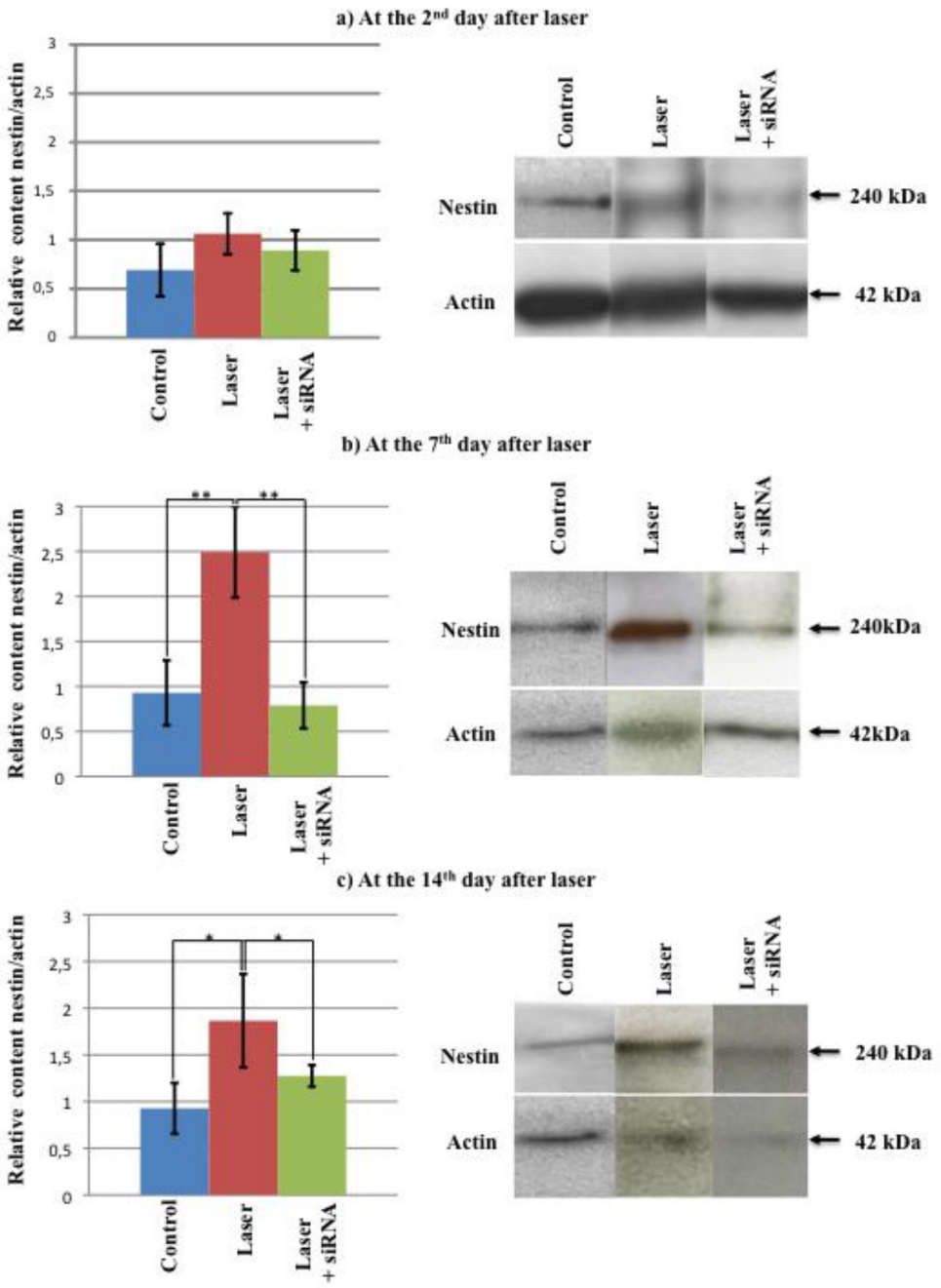

Figure 8. Relative nestin concentrations in the retina at 2, 7, and 14 days after laser treatment. Two days after the laser treatment, no statistically significant increase in nestin expression level was observed. Seven days after the laser treatment, the expression level of nestin was significantly increased. The nestin siRNA injection led to a significant reduction. Fourteen days after the laser treatment, the expression level of nestin remained high, and nestin siRNA injection reduced the intensity of immunoreactivity. Mann-Whitney test, **p < 0.01, *p < 0.05.

[42-45]. After cellular differentiation, nestin is downregulated and replaced by other tissue-specific IF proteins. However, it can be reinduced in adults under pathological conditions [46]. In the adult retina, its presence is reported principally in glial Müller cells after retinal injuries such as retinal detachment [47], optic nerve transection [48], retinitis pigmentosa [49], and laser impact [50].

We investigated the nestin expression in Müller cells after laser beam treatment because it has been hypothesized that some of these cells can dedifferentiate and proliferate in

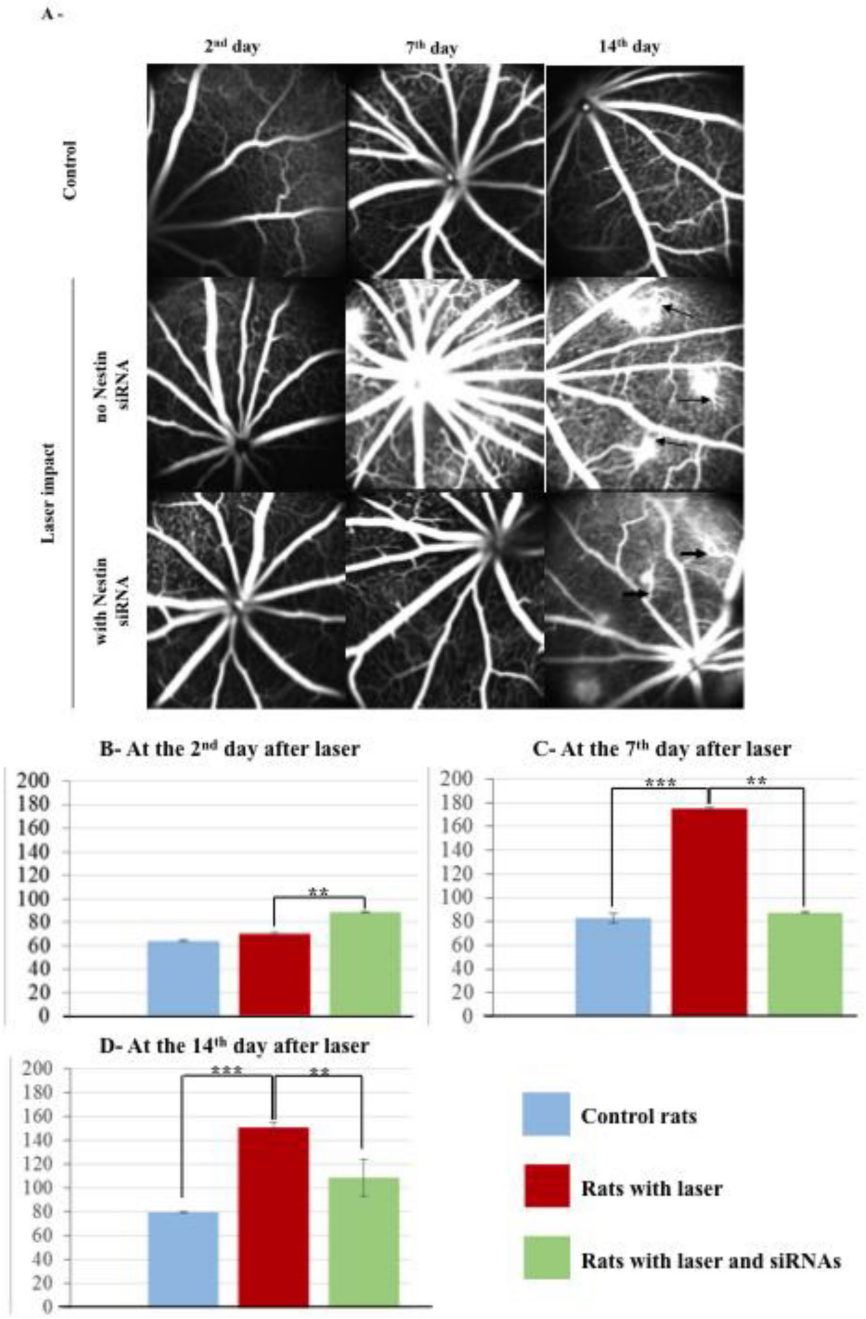

Figure 9. Changes in choroidal vascularization after the laser impacts and nestin siRNA injection. **A**: No apparent changes in vascularization was observed in the control animals during the experimental period (upper panels). On the seventh day after the laser treatment, the angiographic fluorescent intensity increased considerably. On the 14th day, the fluorescence was still intense, with the appearance of dense microvascular networks at the site of the laser impact (upward thin arrow). The nestin siRNA injection reduced the fluorescence intensity, even if some micro-vessel islands were still present on the 14th day (rightward thick arrow). These results are confirmed by the measurement value of the vascular density calculated using the Fiji/Image J analysis software on the **B**: second day, **C**: seventh day, and **D**: 14th day after the laser impacts.

pathological conditions [51]. These cells are known to adapt their shapes and functions to their neuronal environment [52] and to express nestin after the onset of retinal or optic nerve lesions [53]. Elsewhere, K_i-67, a marker for cellular proliferation and cyclin D1, involved in cell cycle progression, has been detected in these cells on the third day after retinochoroidal laser induced-impact [50], which suggests a remodeling of these cells and a possible formation of a matrix-filing-damaged photoreceptor layer [54]. Our results confirm those of Kohno et al., who demonstrated a proliferation of nestin-positive Müller cells after laser injury. However, their study also raised the question of the dedifferentiation and capacity of these cells to become progenitors for retinal cells after laser injury [50]. Our work cannot clearly answer this question, but as reported by Ooto et al. [51], it is probable that some Müller cells constitute a potential source of neural progenitor in adult retina.

The present study demonstrates that numerous radial retinal processes that penetrated into the choroid expressing nestin were present at the site of the lesion from the second day after the laser impacts, suggesting a proliferation and/or resistance to apoptosis of Müller cells. In rats subjected to laser impacts, nestin immunolabeling appeared considerably increased at the site of the lesion after the second day of the laser impact. It was also observed in some parts of blood vessels and in retinal radial processes that penetrated the choroid due to the disruption of the retina caused by the laser impacts. Immunolabeling appeared to increase greatly from the third day and to decrease after the seventh day. These results are in accordance with the reinduction of nestin after the onset of pathological conditions [46]. However, the precise identity of cells containing nestin clearly remains to be defined.

The glial localization of nestin was studied by the coexpression of this protein with glial markers such as GFAP and GS. GFAP is an IF protein specifically expressed in glial cells. In normal retina, it is found only in astrocytes, whereas after retinal stress, it is also expressed in activated Müller cells [55,56]. One function of overexpressed GFAP in injured retina might be to inhibit the extent of the damaged area and to facilitate the transport of molecules required by this damage control process [57]. GFAP appears weakly expressed at the center of the site of the laser impacts on the second day after laser beam delivery, but its expression increased considerably on the third day. Our data are in agreement with the observations of Tackenberg et al. [13], showing that GFAP immunostaining requires at least 48 h after the laser impact to be massively observed, correlating with cell cycle progression. These authors have also demonstrated a local upregulation of the cell cycle markers cyclin D1 and D3 and the migration of activated Müller cell nuclei to the radial processes. However, it is possible that Müller glia reactivity varies according to the type of retinal stress, as GFAP was detected in Müller cells 24 h after *N*-methyl-*N*-nitrosourea (MNU) injection [58]. On the third day after laser beam administration, GFAP immunolabeled processes were also observed in the choroid, confirming the rupture of Bruch's membrane, as previously demonstrated [12]. After the seventh day, GFAP-labeled Müller cell radial processes were found in the retina and choroid, but the penetration into the choroid was reduced (sometimes absent), which suggests the onset of scar formation. On both the seventh and 14th day after the laser impacts, Bruch's membrane remained damaged, but progressive wound healing was confirmed by the scarcity of the radial processes in the choroid. It seems that Müller cell activation finally ends 2 to 4 months after photocoagulation [59], as demonstrated in this study, because we observed that 45 days after the lesion, structural abnormalities persisted in the retina and choroid, and nestin was always detected.

Nestin and GFAP have been proposed as useful biomarkers of retinal injuries [60]. At the level of the laser impacts, the partial coexpression of nestin and GFAP in some radial processes within 3 days after treatment suggests that some Müller cells might undergo transdifferentiation leading to the generation of new retinal neurons, as proposed by Ooto et al. [51] and Takeda et al. [61]. However, Tackenberg et al. [13] refuted this hypothesis, claiming that Müller cell proliferation and migration occurs after laser injury. Nestin-GFAP co-staining is always detected in astrocytes in the GCL in laser-injured and normal retina, which suggests that these cells are constantly engaged in mitotic activity.

GS is also detected in astrocytes and differentiated functional Müller cells [62,63]. In these cells, it transforms glutamate (the principal retinal excitatory neurotransmitter) into glutamine. GS was localized throughout the cytoplasm of the cells in the control and laser-treated animals, indicating continued function despite injury. Despite cellular disorganization and disrupted outer retina and Bruch's membrane, GS is always present in Müller cells confined exclusively within the retina. Nestin/GS coexpression in Müller cells is rarely observed in controls, as in injured retina at early stages after laser injury. From 7 days post injury, partial colocalization was observed in the radial processes, which suggests that the newly created Müller cells could become functionally active. Although mostly expressed in quiescent cells and proliferative neural and glial precursor cells, nestin is also detected in proliferative endothelial cells [30]. We demonstrated that nestin could be involved in angiogenesis [64] because

of it co-immunostaining with vWF. vWF is considered a marker of endothelial cells [65]. It controls angiogenesis and vascular maturation through multiple pathways [66]. As for nestin, vWF immunolabeling appeared to be increased at the lesion site resulting from laser impacts from the second day after laser beam delivery in both the retina and choroid. These results suggest the occurrence of limited and delayed choroidal neovascularization but do not exclude vascular remodeling. The origin of these vessels remains unclear: they may arise from new or redirected vessels or both [12]. Elsewhere, we unequivocally demonstrated that nestin is involved in the proliferation of retinal and choroidal vessels caused by laser impacts. The use of nestin silencing via siRNAs known to inhibit the formation of endothelial cells significantly confirms the involvement of nestin in the formation of vessels [45]. We demonstrated in this study that overexpressed nestin after laser impacts was downregulated after the intraocular injections of chemically synthesized nestin siRNAs, causing reduced blood vessel proliferation, as confirmed on in vivo angiography. Nestin has been observed in proliferative vascular endothelial cells, endothelial progenitors, and tumor-associated neovessels such as those in glioblastoma and prostate, colorectal, pancreatic, breast, and ovarian cancers [67-69]. Thus, nestin seems to be an interesting target against tumors associated with dysregulated angiogenesis. In conclusion, this study shows that nestin appears to play an essential role in the formation and proliferation of endothelial cells and might potentially promote the multiplication of Müller cells after laser impact. This work could orient therapeutic trials targeting wet AMD towards a novel antiangiogenic strategy based on intravitreal injections of specific siRNA blocking nestin overexpression.

APPENDIX 1. HISTOLOGICAL PICTURES OF RETINA AND CHOROID IN RATS AT LASER IMPACT, AT A DISTANCE OF 150MM FROM LASER IMPACT AND WITHOUT KRYPTON LASER IMPACT AT 45TH DAY

To access the data, click or select the words "Appendix 1." Immunofluorescent labeling with DAPI (blue) and nestin (green) is shown. No morphological changes are observed at 150µm from laser impacts and in control rats with no laser impacts, as observed with DAPI staining (A, C). In these conditions, nestin immunostaining is seen in processes of astrocytes and in probable endfeet of Muller cells located mostly in the GCL (horizontal left orientated thin arrow; D). They are also observed in structures similar to blood vessels located in retina and choroid (horizontal large arrows; B D). At the impact, DAPI labeling (E) demonstrated that retinal morphology is greatly disrupted in the outer retina with cells of the ONL entering the choroid (large vertical thick arrow). Nestin immunostaining is observed in glial cells in GCL (thin arrow), in retinal radial processes (horizontal large arrow) and in processes located in choroid (large star; F). All pictures were taken from different retinal sections. GCL: ganglion cell layer, IPL: inner plexiform layer, INL: inner nuclear layer, OPL: outer plexiform layer, ONL: outer nuclear layer, Ch: choroid. Scale bars correspond to 50µm.

ACKNOWLEGMENTS

We would like to thank David Hicks for helpful comments on the manuscript. We also thank Kimberley Delaunay (PhD student in our laboratory) for her help in assessing the number of vessels observed during angiography analysis. This work was supported by INSERM and Paris-Cité University. AUTHOR'S CONTRIBUTION: This work was performed in the collaboration between authors. Author VBC designed the study and wrote the protocol. MS, VM, ESM, and VBC performed the experiments and AM, BCF and VBC wrote the first draft of the manuscript. All authors read and approved the final manuscript. FUNDING INFORMATION: This research program was by an INSERM endowment attributed to the Team 17 of UMR_S INSERM 1138.COMPLIANCE WITH ETHICAL STANDARDS: Everything is disclosed and the work has been ethically performed. CONFLICT OF INTEREST: Professor Francine Behar-Cohen is the major scientific consultant of the Biotechnology Company Eyevensys. The content of this manuscript is completely unrelated to the goals and all types of work performed by Eyevensys. All the other authors declare that they have no conflict of interest.

REFERENCES

1. Constable IJ, Ming S. (1982). Laser, its clinical uses in eye diseases - NLM Catalog -NCBI. https://www.ncbi.nlm.nih.gov/nlmcatalog/9300523.
2. Freund KB, Yannuzzi LA, Sorenson JA. Age-related macular degeneration and choroidal neovascularization. Am J Ophthalmol 1993; 115:786-91. [PMID: 7685148].
3. Schmidt-Erfurth UM, Pruente C. Management of neovascular age-related macular degeneration. Prog Retin Eye Res 2007; 26:437-51. [PMID: 17512238].
4. Virgili G, Bini A. Laser photocoagulation for neovascular age-related macular degeneration. Cochrane Database Syst Rev 2007; CD004763-[PMID: 17636773].
5. Menguy T, Briaux A, Jeunesse E, Giustiniani J, Calcei A, Guyon T, Mizrahi J, Haegel H, Duong V, Soler V, Brousset P, Bensussan A, Raymond Letron I, Le Bouteiller P. Anti-CD160, Alone or in Combination With Bevacizumab, Is a

Potent Inhibitor of Ocular Neovascularization in Rabbit and Monkey Models. Invest Ophthalmol Vis Sci 2018; 59:2687-98. [PMID: 29860455].

6. Miller H, Miller B, Ishibashi T, Ryan SJ. Pathogenesis of laser-induced choroidal subretinal neovascularization. Invest Ophthalmol Vis Sci 1990; 31:899-908. [PMID: 1692312].

7. Favazza TL, Tanimoto N, Munro RJ, Beck SC, Garrido MG, Seide C, Sothilingam V, Hansen RM, Fulton AB, Seeliger MW, Akula JD. Alterations of the tunica vasculosa lentis in the rat model of retinopathy of prematurity. Doc Ophthalmol 2013; 127:3-11. [PMID: 23748796].

8. Miller JW. Age-related macular degeneration revisited–piecing the puzzle: the LXIX Edward Jackson memorial lecture. Am J Ophthalmol 2013; 155:1-35.e13. [PMID: 23245386].

9. Grossniklaus HE, Kang SJ, Berglin L. Animal models of choroidal and retinal neovascularization. Prog Retin Eye Res 2010; 29:500-19. [PMID: 20488255].

10. Chabot S, Jabrane-Ferrat N, Bigot K, Tabiasco J, Provost A, Golzio M, Noman MZ, Giustiniani J, Bellard E, Brayer S, Aguerre-Girr M, Meggetto F, Giuriato S, Malecaze F, Galiacy S, Jaïs JP, Chose O, Kadouche J, Chouaib S, Teissié J, Abitbol M, Bensussan A, Le Bouteiller P. A novel antiangiogenic and vascular normalization therapy targeted against human CD160 receptor. J Exp Med 2011; 208:973-86. Epub 2011 Apr 11[PMID: 21482699].

11. Semkova I, Peters S, Welsandt G, Janicki H, Jordan J, Schraermeyer U. Investigation of laser-induced choroidal neovascularization in the rat. Invest Ophthalmol Vis Sci 2003; 44:5349-54. [PMID: 14638737].

12. Behar-Cohen F, Benezra D, Soubrane G, Jonet L, Jeanny JC. Krypton laser photocoagulation induces retinal vascular remodeling rather than choroidal neovascularization. Exp Eye Res 2006; 83:263-75. [PMID: 16564044].

13. Tackenberg MA, Tucker BA, Swift JS, Jiang C, Redenti S, Greenberg KP, Flannery JG, Reichenbach A, Young MJ. Müller cell activation, proliferation and migration following laser injury. Mol Vis 2009; 15:1886-96. [PMID: 19768129].

14. Vecino E, Rodriguez FD, Ruzafa N, Pereiro X, Sharma SC. Glia-neuron interactions in the mammalian retina. Prog Retin Eye Res 2016; 51:1-40. [PMID: 26113209].

15. Lewis GP, Matsumoto B, Fisher SK. Changes in the organization and expression of cytoskeletal proteins during retinal degeneration induced by retinal detachment. Invest Ophthalmol Vis Sci 1995; 36:2404-16. [PMID: 7591630].

16. Hitchcock P, Ochocinska M, Sieh A, Otteson D. Persistent and injury-induced neurogenesis in the vertebrate retina. Prog Retin Eye Res 2004; 23:183-94. [PMID: 15094130].

17. Abrahan CE, Insua MF, Politi LE, German OL, Rotstein NP. Oxidative stress promotes proliferation and dedifferentiation of retina glial cells in vitro. J Neurosci Res 2009; 87:964-77. [PMID: 18855938].

18. Hosoki A, Oku H, Horie T, Kida T, Sugiyama T, Nakamura K, Ikeda T. Changes in Expression of Nestin, CD44, Vascular Endothelial Growth Factor, and Glutamine Synthetase by Mature Müller Cells After Dedifferentiation. J Ocul Pharmacol Ther 2015; 31:476-81. [PMID: 26091086].

19. Wang L, Li PK. Expressions of nestin and glial fibrillary acidic protein in rat retina after optic nerve transection. Int J Ophthalmol 2017; 10:1510-5. [PMID: 29062768].

20. Xue L, Ding D, Xiao L, Hu M, Hu Z. Nestin, a new marker, expressed in Müller cells following retinal injury. Can J Neurol Sci 2010; 37:643-9. [PMID: 21059512].

21. Lendahl U, Zimmerman LB, McKay RD. CNS stem cells express a new class of intermediate filament protein. Cell 1990; 60:585-95. [PMID: 1689217].

22. Walcott JC, Provis JM. Müller cells express the neuronal progenitor cell marker nestin in both differentiated and undifferentiated human foetal retina. Clin Experiment Ophthalmol 2003; 31:246-9. [PMID: 12786777].

23. Dahlstrand J, Lardelli M, Lendahl U. Nestin mRNA expression correlates with the central nervous system progenitor cell state in many, but not all, regions of developing central nervous system. Brain Res Dev Brain Res 1995; 84:109-29. [PMID: 7720210].

24. Turner DL, Snyder EY, Cepko CL. Lineage-independent determination of cell type in the embryonic mouse retina. Neuron 1990; 4:833-45. [PMID: 2163263].

25. Dahlstrand J, Collins VP, Lendahl U. Expression of the class VI intermediate filament nestin in human central nervous system tumors. Cancer Res 1992; 52:5334-41. [PMID: 1382841].

26. Osman WM, Shash LS, Ahmed NS. Emerging Role of Nestin as an Angiogenesis and Cancer Stem Cell Marker in Epithelial Ovarian Cancer: Immunohistochemical Study. Appl Immunohistochem Mol Morphol 2017; 25:571-80. [PMID: 26945442].

27. Mokrý J, Cízková D, Filip S, Ehrmann J, Osterreicher J, Kolàr Z, English D. Nestin expression by newly formed human blood vessels. Stem Cells Dev 2004; 13:658-64. [PMID: 15684833].

28. Aihara M, Sugawara K, Torii S, Hosaka M, Kurihara H, Saito N, Takeuchi T. Angiogenic endothelium-specific nestin expression is enhanced by the first intron of the nestin gene. Lab Invest 2004; 84:1581-92. [PMID: 15502861].

29. Shimizu T, Sugawara K, Tosaka M, Imai H, Hoya K, Takeuchi T, Sasaki T, Saito N. Nestin expression in vascular malformations: a novel marker for proliferative endothelium. Neurol Med Chir (Tokyo) 2006; 46:111-7. [PMID: 16565580].

30. Teranishi N, Naito Z, Ishiwata T, Tanaka N, Furukawa K, Seya T, Shinji S, Tajiri T. Identification of neovasculature using nestin in colorectal cancer. Int J Oncol 2007; 30:593-603. [PMID: 17273760].

31. Amarzguioui M, Lundberg P, Cantin E, Hagstrom J, Behlke MA, Rossi JJ. Rational design and in vitro and in vivo delivery of Dicer substrate siRNA. Nat Protoc 2006; 1:508-17. [PMID: 17406276].

32. Schindelin J, Arganda-Carreras I, Frise E, Kaynig V, Longair M, Pietzsch T, Preibisch S, Rueden C, Saalfeld S, Schmid B,

Tinevez JY, White DJ, Hartenstein V, Eliceiri K, Tomancak P, Cardona A. Fiji: an open-source platform for biological-image analysis. Nat Methods 2012; 9:676-82. [PMID: 22743772].

33. Eliasson C, Sahlgren C, Berthold CH, Stakeberg J, Celis JE, Betsholtz C, Eriksson JE, Pekny M. Intermediate filament protein partnership in astrocytes. J Biol Chem 1999; 274:23996-4006. [PMID: 10446168].

34. Takamori Y, Mori T, Wakabayashi T, Nagasaka Y, Matsuzaki T, Yamada H. Nestin-positive microglia in adult rat cerebral cortex. Brain Res 2009; 1270:10-8. [PMID: 19306852].

35. Shen Q, Zhong W, Jan YN, Temple S. Asymmetric Numb distribution is critical for asymmetric cell division of mouse cerebral cortical stem cells and neuroblasts. Development 2002; 129:4843-53. [PMID: 12361975].

36. Bieberich E, MacKinnon S, Silva J, Noggle S, Condie BG. Regulation of cell death in mitotic neural progenitor cells by asymmetric distribution of prostate apoptosis response 4 (PAR-4) and simultaneous elevation of endogenous ceramide. J Cell Biol 2003; 162:469-79. [PMID: 12885759].

37. Sahlgren CM, Mikhailov A, Vaittinen S, Pallari HM, Kalimo H, Pant HC, Eriksson JE. Cdk5 regulates the organization of Nestin and its association with p35. Mol Cell Biol 2003; 23:5090-106. [PMID: 12832492].

38. Toivola DM, Tao G-Z, Habtezion A, Liao J, Omary MB. Cellular integrity plus: organelle- related and protein-targeting functions of intermediate filaments. Trends Cell Biol 2005; 15:608-17. [PMID: 16202602].

39. Sunabori T, Tokunaga A, Nagai T, Sawamoto K, Okabe M, Miyawaki A, Matsuzaki Y, Miyata T, Okano H. Cell-cycle-specific nestin expression coordinates with morphological changes in embryonic cortical neural progenitors. J Cell Sci 2008; 121:1204-12. [PMID: 18349072].

40. Sahlgren CM, Pallari H-M, He T, Chou Y-H, Goldman RD, Eriksson JE. A nestin scaffold links Cdk5/p35 signaling to oxidant-induced cell death. EMBO J 2006; 25:4808-19. [PMID: 17036052].

41. Chen H-L, Yuh C-H, Wu KK. Nestin is essential for zebrafish brain and eye development through control of progenitor cell apoptosis. PLoS One 2010; 5:e9318-[PMID: 20174467].

42. Sahlgren CM, Mikhailov A, Hellman J, Chou YH, Lendahl U, Goldman RD, Eriksson JE. Mitotic reorganization of the intermediate filament protein nestin involves phosphorylation by cdc2 kinase. J Biol Chem 2001; 276:16456-63. [PMID: 11278541].

43. Wiese C, Rolletschek A, Kania G, Navarrete-Santos A, Anisimov SV, Steinfarz B, Tarasov KV, Brugh SA, Zahanich I, Ruschenschmidt C, Beck H, Blyszczuk P, Czyz J, Heubach JF, Ravens U, Horstmann O, St-Onge L, Braun T, Brustle O, Boheler KR, Wobus AM. Signals from embryonic fibroblasts induce adult intestinal epithelial cells to form nestin-positive cells with proliferation and multilineage differentiation capacity in vitro. Stem Cells 2006; 24:2085-97. [PMID: 16741226].

44. Daniel C, Albrecht H, Lüdke A, Hugo C. Nestin expression in repopulating mesangial cells promotes their proliferation. Lab Invest 2008; 88:387-97. [PMID: 18268475].

45. Liang Z-W, Wang Z, Chen H, Li C, Zhou T, Yang Z, Yang X, Yang Y, Gao G, Cai W. Nestin-mediated cytoskeletal remodeling in endothelial cells: novel mechanistic insight into VEGF-induced cell migration in angiogenesis. Am J Physiol Cell Physiol 2015; 308:C349-58. [PMID: 25500739].

46. Douen AG, Dong L, Vanance S, Munger R, Hogan MJ, Thompson CS, Hakim AM. Regulation of nestin expression after cortical ablation in adult rat brain. Brain Res 2004; 1008:139-46. [PMID: 15145750].

47. Luna G, Lewis GP, Banna CD, Skalli O, Fisher SK. Expression profiles of nestin and synemin in reactive astrocytes and Müller cells following retinal injury: a comparison with glial fibrillar acidic protein and vimentin. Mol Vis 2010; 16:2511-23. [PMID: 21139996].

48. Xue LP, Lu J, Cao Q, Hu S, Ding P, Ling EA. Müller glial cells express nestin coupled with glial fibrillary acidic protein in experimentally induced glaucoma in the rat retina. Neuroscience 2006; 139:723-32. https:// doi.org[PMID: 16458441].

49. Valamanesh F, Monnin J, Morand-Villeneuve N, Michel G, Zaher M, Miloudi S, Chemouni D, Jeanny JC, Versaux-Botteri C. Nestin expression in the retina of rats with inherited retinal degeneration. Exp Eye Res. 2013 May;110:26–34. https://doi: 10.1016/j.exer.2013.01.01310.1016/j.exer.2013.01.013

50. Kohno H, Sakai T, Kitahara K. Induction of nestin, Ki-67, and cyclin D1 expression in Müller cells after laser injury in adult rat retina. Graefes Arch Clin Exp Ophthalmol 2006; 244:90-5. [PMID: 15983812].

51. Ooto S. Potential for neural regeneration in the adult mammalian retina. Nippon Ganka Gakkai Zasshi 2006; 110:864-71. [PMID: 17134034].

52. Newman E, Reichenbach A. The Müller cell: a functional element of the retina. Trends Neurosci 1996; 19:307-12. [PMID: 8843598].

53. Wohl SG, Schmeer CW, Kretz A, Witte OW, Isenmann S. Optic nerve lesion increases cell proliferation and nestin expression in the adult mouse eye in vivo. Exp Neurol 2009; 219:175-86. [PMID: 19445936].

54. Dot C, Behar-Cohen F, BenEzra D, Doat M, Jonet L, May F, Jeanny JC. Influence of triamcinolone intravitreal injection on retinochoroidal healing processes. Exp Eye Res 2007; 84:1081-9. [PMID: 17408616].

55. Grosche J, Härtig W, Reichenbach A. Expression of glial fibrillary acidic protein (GFAP), glutamine synthetase (GS), and Bcl-2 protooncogene protein by Müller (glial) cells in retinal light damage of rats. Neurosci Lett 1995; 185:119-22. [PMID: 7746501].

56. Humphrey MF, Chu Y, Mann K, Rakoczy P. Retinal GFAP and bFGF expression after multiple argon laser photocoagulation injuries assessed by both immunoreactivity and mRNA levels. Exp Eye Res 1997; 64:361-9. [PMID: 9196387].

57. Eng LF, Ghirnikar RS, Lee YL. Glial fibrillary acidic protein: GFAP-thirty-one years (1969–2000). Neurochem Res 2000; 25:1439-51. [PMID: 11059815].

58. Moon CH, Cho H, Kim YK, Park TK. Nestin Expression in the Adult Mouse Retina with Pharmaceutically Induced Retinal Degeneration. J Korean Med Sci 2017; 32:343-51. [PMID: 28049248].

59. Sher A, Jones BW, Huie P, Paulus YM, Lavinsky D, Leung L-SS, Nomoto H, Beier C, Marc RE, Palanker D. Restoration of retinal structure and function after selective photocoagulation. J Neurosci 2013; 33:6800-8. [PMID: 23595739].

60. Xue LP, Lu J, Cao Q, Hu S, Ding P, Ling E-A. Müller glial cells express nestin coupled with glial fibrillary acidic protein in experimentally induced glaucoma in the rat retina. Neuroscience 2006; 139:723-32. [PMID: 16458441].

61. Takeda M, Takamiya A, Jiao J-W, Cho K-S, Trevino SG, Matsuda T, Chen DF. alpha-Aminoadipate induces progenitor cell properties of Müller glia in adult mice. Invest Ophthalmol Vis Sci 2008; 49:1142-50. [PMID: 18326742].

62. Riepe RE, Norenburg MD. Müller cell localisation of glutamine synthetase in rat retina. Nature 1977; 268:654-5. [PMID: 19708].

63. Derouiche A, Rauen T. Coincidence of L-glutamate/L-aspartate transporter (GLAST) and glutamine synthetase (GS) immunoreactions in retinal glia: evidence for coupling of GLAST and GS in transmitter clearance. J Neurosci Res 1995; 42:131-43. [PMID: 8531222].

64. Suzuki S, Namiki J, Shibata S, Mastuzaki Y, Okano H. The neural stem/progenitor cell marker nestin is expressed in proliferative endothelial cells, but not in mature vasculature. J Histochem Cytochem 2010; 58:721-30. [PMID: 20421592].

65. Peyvandi F, Garagiola I, Baronciani L. Role of von Willebrand factor in the haemostasis. Blood Transfus 2011; 9:Suppl 2s3-8. [PMID: 21839029].

66. Randi AM, Laffan MA. Von Willebrand factor and angiogenesis: basic and applied issues. J Thromb Haemost 2017; 15:13-20. [PMID: 27778439].

67. Matsuda Y, Masahito Hagio M, Ishiwata T. Nestin: a novel angiogenesis marker and possible target for tumor angiogenesis. World J Gastroenterol 2013; 19:42-8. [PMID: 23326161].

68. Czekierdowski A, Stachowicz N, Czekierdowska S, Łoziński T, Gurynowicz G, Kluz T, Stachowicz N, Czekierdowska S, Łoziński T, Gurynowicz G, Kluz T. Prognostic significance of TEM7 and nestin expression in women with advanced high grade serous ovarian cancer. Ginekol Pol 2018; 89:135-41. [PMID: 29664548].

69. Nowak A, Grzegrzółka J, Kmiecik A, Piotrowska A, Matkowski R, Dzięgiel P. Role of nestin expression in angiogenesis and breast cancer progression. Int J Oncol 2018; 52:527-35. [PMID: 29345290].

Articles are provided courtesy of Emory University and the Zhongshan Ophthalmic Center, Sun Yat-sen University, P.R. China. The print version of this article was created on 4 September 2022. This reflects all typographical corrections and errata to the article through that date. Details of any changes may be found in the online version of the article.